Datasheet for 600-901-379S

RFP Antibody

Overview

Description:	Anti-RFP (CHICKEN) Antibody - 600-901-379S
Item No.:	600-901-379S
Size:	25 µL
Applications:	ELISA, WB, FC, IF, IHC, Multiplex
Reactivity:	RFP, rRFP, tdTomato
Host Species:	Chicken

Product Details

Background:	Fluorescent proteins such as Discosoma Red Fluorescent Protein (DsRed) from sea anemone Discosoma sp. mushroom or green fluorescent protein (GFP) from Aequorea victoria jellyfish are widely used in research practice. Fusion RFP and GFP commonly serve as marker for gene expression and protein localization. As DsRed and GFP share only 19% identity, therefore, in general, anti-GFP antibodies do not recognize DsRed protein and vice versa. Structurally, Discosoma red fluorescent protein is similar to Aequorea green fluorescent protein in terms of its overall fold (a β-can) and chromophore-formation chemistry. However, Discosoma red fluorescent protein undergoes an additional step in the chromophore maturation and obligates tetrameric structure. Rockland offers many controls, monoclonal, and polyclonal antibodies for RFP.
Synonyms:	chicken anti-RFP antibody, DsRed, rDsRed, Discosoma sp. Red Fluorescent Protein, Red fluorescent protein drFP583
Host Species:	Chicken
Clonality:	Polyclonal
Format:	IgY

Target Details

Gene Name:	DsRed
Reactivity:	RFP, rRFP, tdTomato
Immunogen Type:	Recombinant Protein

Immunogen:	Red Fluorescent Protein (RFP) fusion protein corresponding to the full length amino acid sequence (234aa) derived from the mushroom polyp coral Discosoma.
Purity/Specificity:	RFP Antibody was prepared from egg yolks by a multi-step process which includes filtration, delipidation, salt fractionation and extensive dialysis against the buffer stated above. RFP Antibody was tested by western blot.
Relevant Links:	• UniProtKB - Q9U6Y8 • 600-901-379 SDS

Application Details

Tested Applications:	ELISA, WB
Suggested Applications:	FC, IF, IHC, Multiplex (Based on references)
Application Note:	Anti-RFP is designed to detect recombinant RFP. Anti-RFP antibody has been tested by ELISA and western blot to detect RFP. Use either alkaline phosphatase or peroxidase conjugated polyclonal anti-RFP to detect RFP or RFP containing proteins on western blots. Optimal titers for applications should be determined by the researcher. This product shows optimal performance by western blot.
Assay Dilutions:	All assays should be optimized by the user. Recommended dilutions (if any) may be listed below.
ELISA:	1:10,000
WB:	1:2,000 - 1:3,000

Formulation

Physical State:	Liquid (sterile filtered)
Concentration:	1.05 mg/mL by UV absorbance at 280 nm
Buffer:	0.02 M Potassium Phosphate, 0.15 M Sodium Chloride, pH 7.2
Preservative:	0.01% (w/v) Sodium Azide
Stabilizer:	None

Shipping & Handling

Shipping Condition:	Dry Ice

Storage Condition:	Store vial at -20° C or below prior to opening. This vial contains a relatively low volume of reagent (25 µL). To minimize loss of volume dilute 1:10 by adding 225 µL of the buffer stated above directly to the vial. Recap, mix thoroughly and briefly centrifuge to collect the volume at the bottom of the vial. Use this intermediate dilution when calculating final dilutions as recommended below. Store the vial at -20°C or below after dilution. Avoid cycles of freezing and thawing.
Expiration:	Expiration date is three (3) months from date of receipt.

Images

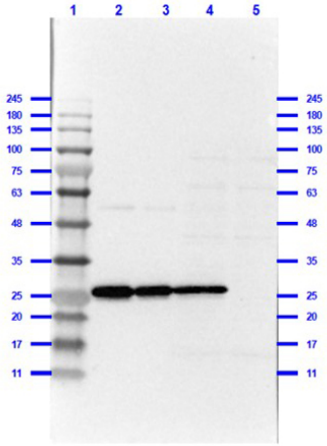

Western Blot
Western Blot of Chicken Anti-RFP Antibody.
Lane 1: Prestained MW marker (p/n MB-210-0500).
Lane 2: RFP (p/n 000-001-379) 0.1µg reduced [+].
Lane 3: RFP (p/n 000-001-379) 0.05µg reduced [+].
Lane 4: RFP/HEK293T (p/n 000-001-379/W09-001-GX5) 0.5µg/10µg reduced [+].
Lane 5: HEK293T (p/n W09-001-GX5) 10µg reduced [-].
Blocking Buffer: BlockOut® Universal Blocking Buffer (p/n MB-073) for 1hr at RT.
Primary Antibody: Chicken Anti-RFP at 1µg/mL overnight at 2-8°C.
Secondary Antibody: Rabbit anti-Chicken IgG HRP (p/n 603-4302) at 1:40,000 for 30 mins at RT.
Predicted/Observed: 27kda.

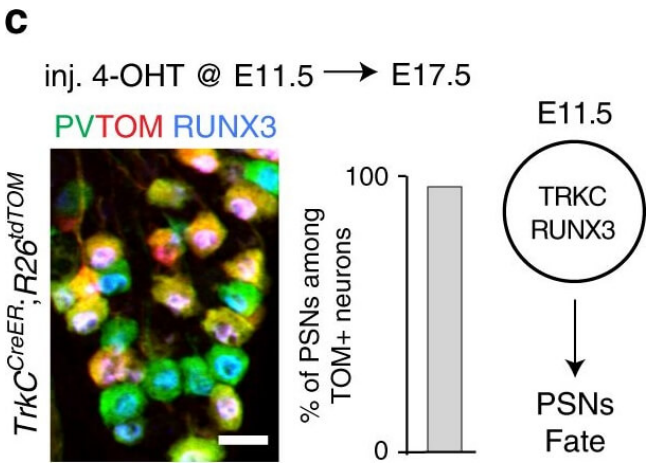

Immunocytochemistry

Differential expression of TRKC in PSNs prior to the cell death period. a Scheme of our working hypothesis. b, c Temporal fate mapping of TRKC PSNs by 4-OHT induction. TrkCCreER mice allow temporary activation of CreER in the TRKC+ cells 2 h after 4-OHT injection21,22. Immunostaining for PV, RFP and RUNX3 on E17.5 DRG sections (c) and graph showing distribution of PV+/RUNX3+ PSNs among the TOM+ cells (n = 4). Scale bar: 20 µm. d Quantification of PSNs at C5 and C7. ***P < 0.001, one-way analysis of variance (ANOVA) with Sidak's multiple comparisons test (n = 2–3). The window of PSNs cell death is shown. e TRKC expression in E11.5 ISL1+ (and RUNX3+, whose staining is not shown for more visibility) DRG neurons. Scale bar: 50 µm. f TRKC levels in PSNs of e illustrated by color coding; dark blue indicates the lower and red the higher TRKC levels. From here, all observations are done at brachial levels (C5–8). g Distribution of TRKC levels in PSNs from e. h Distribution of TRKC levels in PSNs in E11.5 DRG neurons (from g). The data exhibit a Poisson-like distribution (one representative animal), with the mean used to define the two different categories of TRKC intensity (TRKCHigh and TRKCLow). i Projection of seven images of RUNX3+/TRKC+ PSNs from one brachial DRG; dots indicate TRKC-labeled neurons and color codes reveal TRKC intensity as shown in h. j Projection image of smFISH for pan Ntrk3 and Ntrk3 full length (FL) transcripts in E11.5 DRG, visualized at high magnification in (1) and (2) (images show full projection); right panel shows color coding of Ntrk3 FL levels in red; the brighter, the higher levels. k Distribution of the number of Ntrk3 FL molecules in E11.5 DRG neurons by smFISH, normalized to pan Ntrk3 (Ntrk3 FL represent 68% of all Ntrk3 transcripts). lTrkCCreER;R26tdTOM mice were injected at E9.75 with 4-OHT and analyzed at E11.5 (n = 3). m, n Frequency distribution (m) and pie chart (n) of TOM+/TRKC+ neurons from l according to their level of TRKC intensity. Source data are available as a Source Data file Figure provided by CiteAb. Source: Nat Commun, PMID: 31515492.

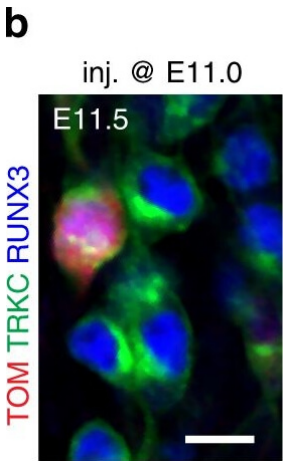

Immunocytochemistry

PSNs with high TRKC levels preferentially survive the cell death period. a Temporal fate mapping of TRKCHigh PSNs by 4-OHT (low dose, 0.02 g/kg). b–d Injection of TrkCCreER;R26tdTOM mice with low dose of 4-OHT at E11.0; DRG analyzed at E11.5 with recombination in few (b), preferentially high TRKC PSNs (c, d) ($P < 0.001$). Frequency distribution of TOM+ PSNs according to TRKC intensity (c) and pie charts (d) illustrating the large proportion of TOM+ cells among TRKCHigh PSNs. Scale bar: 50 µm. e, f Percentage of recombined PSNs at E11.5 and E13.5 in DRGs from TrkCCreER;R26tdTOM animals after 4-OHT injection at E11.0 (*$P < 0.05$, Student's t-test; n = 2 litters with 6 embryos, E11.5; 2 litters with 5 embryos, E13.5). g The percentage of labeled PSNs does not change between E11.5 and E13.5 in R26CreERT2;R26tdTOM embryos injected at E11.0 with 0.032 g/kg 4-OHT (n = 4). Similarly, the recombination rate in TOM+ PSNs does not change between E14.5 and E16.5 in TrkCCreER;R26tdTOM embryos after injection at E14.0 with 0.02 g/kg 4-OHT (n = 2). Unpaired Student's t-test. h Whole-mount immunostaining for TRKC, NF160 and RFP of E13.5 forelimb from TrkCCreER;R26tdTOM embryos injected with low dose 4-OHT at E11.0. Insert shows restricted number of TOM+ fibers dispersed amongst TRKC+ axons. Scale bar: 200 µm. i Pattern and color-coded depth (in micrometers) of innervation of TRKC+, NF160+ and RFP+ nerve fibers (processed from h) of E13.5 forelimb from TrkCCreER;R26tdTOM embryos injected with a low dose of 4-OHT (0.02 g/kg) at E11. The pattern and depth color code reveal similar territories (in all dimensions, xyz) of innervation of the TOM+ PSNs compared to all axons (NF160). Scale bar: 200 µm. j Scheme illustrating the preferential selection of TRKCHigh PSNs during the cell death period. Source data are available as a Source Data file Figure provided by CiteAb. Source: Nat Commun, PMID: 31515492.

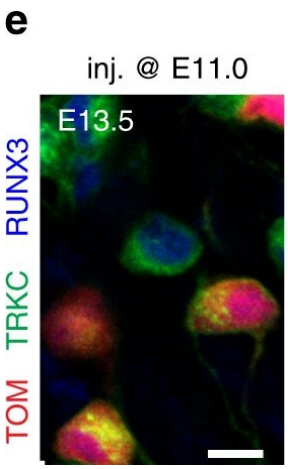

Immunocytochemistry

PSNs with high TRKC levels preferentially survive the cell death period. a Temporal fate mapping of TRKCHigh PSNs by 4-OHT (low dose, 0.02 g/kg). b–d Injection of TrkCCreER;R26tdTOM mice with low dose of 4-OHT at E11.0; DRG analyzed at E11.5 with recombination in few (b), preferentially high TRKC PSNs (c, d) ($P < 0.001$). Frequency distribution of TOM+ PSNs according to TRKC intensity (c) and pie charts (d) illustrating the large proportion of TOM+ cells among TRKCHigh PSNs. Scale bar: 50 µm. e, f Percentage of recombined PSNs at E11.5 and E13.5 in DRGs from TrkCCreER;R26tdTOM animals after 4-OHT injection at E11.0 (*$P < 0.05$, Student's t-test; n = 2 litters with 6 embryos, E11.5; 2 litters with 5 embryos, E13.5). g The percentage of labeled PSNs does not change between E11.5 and E13.5 in R26CreERT2;R26tdTOM embryos injected at E11.0 with 0.032 g/kg 4-OHT (n = 4). Similarly, the recombination rate in TOM+ PSNs does not change between E14.5 and E16.5 in TrkCCreER;R26tdTOM embryos after injection at E14.0 with 0.02 g/kg 4-OHT (n = 2). Unpaired Student's t-test. h Whole-mount immunostaining for TRKC, NF160 and RFP of E13.5 forelimb from TrkCCreER;R26tdTOM embryos injected with low dose 4-OHT at E11.0. Insert shows restricted number of TOM+ fibers dispersed amongst TRKC+ axons. Scale bar: 200 µm. i Pattern and color-coded depth (in micrometers) of innervation of TRKC+, NF160+ and RFP+ nerve fibers (processed from h) of E13.5 forelimb from TrkCCreER;R26tdTOM embryos injected with a low dose of 4-OHT (0.02 g/kg) at E11. The pattern and depth color code reveal similar territories (in all dimensions, xyz) of innervation of the TOM+ PSNs compared to all axons (NF160). Scale bar: 200 µm. j Scheme illustrating the preferential selection of TRKCHigh PSNs during the cell death period. Source data are available as a Source Data file Figure provided by CiteAb. Source: Nat Commun, PMID: 31515492.

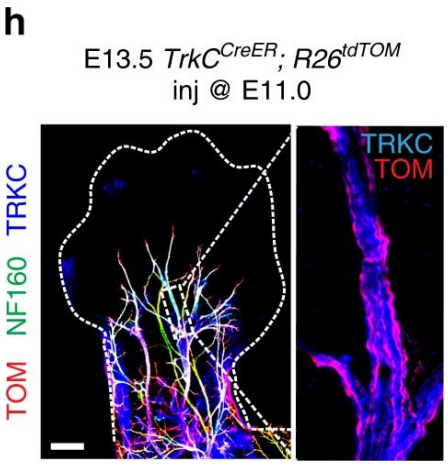

Immunohistochemistry

PSNs with high TRKC levels preferentially survive the cell death period. a Temporal fate mapping of TRKCHigh PSNs by 4-OHT (low dose, 0.02 g/kg). b–d Injection of TrkCCreER;R26tdTOM mice with low dose of 4-OHT at E11.0; DRG analyzed at E11.5 with recombination in few (b), preferentially high TRKC PSNs (c, d) ($P < 0.001$). Frequency distribution of TOM+ PSNs according to TRKC intensity (c) and pie charts (d) illustrating the large proportion of TOM+ cells among TRKCHigh PSNs. Scale bar: 50 µm. e, f Percentage of recombined PSNs at E11.5 and E13.5 in DRGs from TrkCCreER;R26tdTOM animals after 4-OHT injection at E11.0 (*$P < 0.05$, Student's t-test; n = 2 litters with 6 embryos, E11.5; 2 litters with 5 embryos, E13.5). g The percentage of labeled PSNs does not change between E11.5 and E13.5 in R26CreERT2;R26tdTOM embryos injected at E11.0 with 0.032 g/kg 4-OHT (n = 4). Similarly, the recombination rate in TOM+ PSNs does not change between E14.5 and E16.5 in TrkCCreER;R26tdTOM embryos after injection at E14.0 with 0.02 g/kg 4-OHT (n = 2). Unpaired Student's t-test. h Whole-mount immunostaining for TRKC, NF160 and RFP of E13.5 forelimb from TrkCCreER;R26tdTOM embryos injected with low dose 4-OHT at E11.0. Insert shows restricted number of TOM+ fibers dispersed amongst TRKC+ axons. Scale bar: 200 µm. i Pattern and color-coded depth (in micrometers) of innervation of TRKC+, NF160+ and RFP+ nerve fibers (processed from h) of E13.5 forelimb from TrkCCreER;R26tdTOM embryos injected with a low dose of 4-OHT (0.02 g/kg) at E11. The pattern and depth color code reveal similar territories (in all dimensions, xyz) of innervation of the TOM+ PSNs compared to all axons (NF160). Scale bar: 200 µm. j Scheme illustrating the preferential selection of TRKCHigh PSNs during the cell death period. Source data are available as a Source Data file Figure provided by CiteAb. Source: Nat Commun, PMID: 31515492.

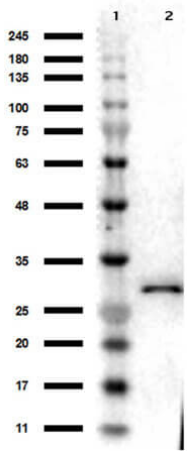

Western Blot
Western Blot Results of Chicken Anti-RFP Antibody. Lane 1: Opal PreStained Molecular Weight Marker (p/n MB-210-0500). Lane 2: RFP (p/n 000-001-379), load 50ng. Primary Antibody: Anti-RFP 1µg/mL overnight at 4°C. Secondary Antibody: Goat Anti-Chicken HRP (p/n 603-103-126) at 1:40,000 for 30min at RT. Blocking: BlockOut (p/n MB-073) for 30min at RT. Expect: 27kDa.

References

- Ibrahimi, M et al. TRACR: an anterograde transneuronal tracing system for genetic access across synapses and longitudinal circuit analysis. *BioRxiv [Preprint]* (2026)
- Bjorklund GR et al. Hyperactivation of MEK1 in cortical glutamatergic neurons results in projection axon deficits and aberrant motor learning. *Dis Model Mech.* (2024)
- Yap KK et al. Liver specification of human iPSC-derived endothelial cells transplanted into mouse liver. *JHEP Rep.* (2024)
- Chen H et al. The functional and anatomical characterization of three spinal output pathways of the anterolateral tract. *Cell Rep.* (2024)
- Ishihara T et al. Meflin/ISLR is a marker of adipose stem and progenitor cells in mice and humans that suppresses white adipose tissue remodeling and fibrosis. *Genes Cells.* (2024)
- Sharma A et al. Mitochondrial Bioenergetics of Functional Wound Closure is Dependent on Macrophage-Keratinocyte Exosomal Crosstalk. *ACS Nano.* (2024)
- Benevento M et al. A brainstem-hypothalamus neuronal circuit reduces feeding upon heat exposure. *Nature.* (2024)
- Stern DB et al. Anatomical Connectivity of the Intercalated Cells of the Amygdala. *eNeuro.* (2023)
- Lark ARS et al. Progressive Degeneration and Adaptive Excitability in Dopamine D1 and D2 Receptor-Expressing Striatal Neurons Exposed to HIV-1 Tat and Morphine. *Cell Mol Neurobiol.* (2023)
- Chapman TW et al. Oligodendrocyte death initiates synchronous remyelination to restore cortical myelin patterns in mice. *Nat Neurosci.* (2023)
- Tan CX et al. δ-Catenin controls astrocyte morphogenesis via layer-specific astrocyte-neuron cadherin interactions. *J Cell Biol.* (2023)
- Vinopal S et al. Centrosomal microtubule nucleation regulates radial migration of projection neurons independently of polarization in the developing brain. *Neuron.* (2023)

- Reyes EA et al. Epithelial TNF controls cell differentiation and CFTR activity to maintain intestinal mucin homeostasis. *J Clin Invest.* (2023)
- Huang XT et al. Embryogenic stem cell-derived intestinal crypt fission directs de novo crypt genesis. *Cell Rep.* (2022)
- Dietschi Q et al. Clustering of vomeronasal receptor genes is required for transcriptional stability but not for choice. *Sci Adv.* (2022)
- Xie Y et al. Astrocyte-neuron crosstalk through Hedgehog signaling mediates cortical synapse development. *Cell Rep.* (2022)
- Qi J et al. Posteromedial thalamic nucleus activity significantly contributes to perceptual discrimination. *PLoS Biol.* (2022)
- Campbell LA et al. Protein-retention expansion microscopy for visualizing subcellular organelles in fixed brain tissue. *J Neurosci Methods.* (2021)
- Nestor-Kalinoski A et al. Unique neural circuit connectivity of mouse proximal, middle, and distal colon defines regional colonic motor patterns. *Cell Mol Gastroenterol Hepatol.* (2021)
- Garcia MT et al. Transcriptional profiling of sequentially generated septal neuron fates. *Elife.* (2021)
- Baldwin KT et al. HepaCAM controls astrocyte self-organization and coupling. *Neuron.* (2021)
- Chipman PH et al. Astrocyte GluN2C NMDA receptors control basal synaptic strengths of hippocampal CA1 pyramidal neurons in the stratum radiatum. *Elife.* (2021)
- Wu H et al. Distinct subtypes of proprioceptive dorsal root ganglion neurons regulate adaptive proprioception in mice. *Nature Communications.* (2021)
- Hara A et al. Meflin defines mesenchymal stem cells and/or their early progenitors with multilineage differentiation capacity. *Genes Cells.* (2021)
- Roth E et al. Behavioural and neurochemical mechanisms underpinning the feeding-suppressive effect of GLP-1/CCK combinatorial therapy. *Mol Metab.* (2021)
- Trebels, B et al. Metamorphic development of the olfactory system in the red flour beetle (Tribolium castaneum, HERBST). *Bmc Biology* (2021)
- Stevens, L et al. Optimized Parameters for Transducing the Locus Coeruleus Using Canine Adenovirus Type 2 (CAV2) Vector in Rats for Chemogenetic Modulation Research. *Frontiers in Neuroscience* (2021)
- Faure, L et al. Single cell RNA sequencing identifies early diversity of sensory neurons forming via bi-potential intermediates. *Nature Communications* (2020)
- Murata, Y et al. GABAergic interneurons excite neonatal hippocampus in vivo. *Science Advances* (2020)
- Harris, JM et al. Long-Range Optogenetic Control of Axon Guidance Overcomes Developmental Boundaries and Defects. *Developmental Cell* (2020)
- Stevens, L et al. A Feasibility Study to Investigate Chemogenetic Modulation of the Locus Coeruleus by Means of Single Unit Activity. *Frontiers in Neuroscience* (2020)
- Shibata-Germanos S, Goodman JR, Grieg A, et al. Structural and functional conservation of non-lumenized lymphatic endothelial cells in the mammalian leptomeninges. *Acta Neuropathol.* (2020)

- Di Matteo F, Pipicelli F, Kyrousi C, et al. Cystatin B is essential for proliferation and interneuron migration in individuals with EPM1 epilepsy. *EMBO Mol Med.* (2020)
- Padmashri R, Ren B, Oldham B, Jung Y, Gough R, Dunaevsky A. Modeling Human-specific Interlaminar Astrocytes in the Mouse Cerebral Cortex. *J Comp Neurol.* (2020)
- Chen PY et al. Smooth muscle cell reprogramming in aortic aneurysms. *Cell Stem Cell.* (2020)
- Goodson NB et al. Simultaneous deletion of Prdm1 and Vsx2 enhancers in the retina alters photoreceptor and bipolar cell fate specification, yet differs from deleting both genes. *Development.* (2020)
- Goodson NB et al. Prdm1 overexpression causes a photoreceptor fate-shift in nascent, but not mature, bipolar cells. *Dev Biol.* (2020)
- DeSisto J et al. Single-cell transcriptomic analyses of the developing meninges reveal meningeal fibroblast diversity and function. *Dev Cell.* (2020)
- Trebels, B., Dippel, S., Schaaf, M. et al. Adult neurogenesis in the mushroom bodies of red flour beetles (Tribolium castaneum, HERBST) is influenced by the olfactory environment. *Sci Rep* (2020)
- Cassandras M et al. Gli1+ mesenchymal stromal cells form a pathological niche to promote airway progenitor metaplasia in the fibrotic lung. *Nat Cell Biol.* (2020)
- Alizzi RA et al. The ELAV/Hu protein Found in neurons regulates cytoskeletal and ECM adhesion inputs for space-filling dendrite growth. *PLoS Genet.* (2020)
- Torre-Muruzabal, T et al. Chronic nigral neuromodulation aggravates behavioral deficits and synaptic changes in an α-synuclein based rat model for Parkinson's disease. *Acta Neuropathologica Communications* (2019)
- Wang Y et al. A cell fitness selection model for neuronal survival during development. *Nat Commun.* (2019)
- Drake KA, Fessler AR, Carroll TJ. Methods for renal lineage tracing: In vivo and beyond. *Methods Cell Biol.* (2019)
- Pignatelli M, Ryan TJ, Roy DS, et al. Engram Cell Excitability State Determines the Efficacy of Memory Retrieval. *Neuron.* (2019)
- Korrell KV, Disser J, Parley K, et al. Differential effect on myelination through abolition of activity-dependent synaptic vesicle release or reduction of overall electrical activity of selected cortical projections in the mouse. *J Anat.* (2019)
- Kim D, An H, Shearer RS, et al. A principled strategy for mapping enhancers to genes. *Sci Rep.* (2019)
- Ko KI, Syverson AL, Kralik RM, et al. Diabetes-Induced NF-κB Dysregulation in Skeletal Stem Cells Prevents Resolution of Inflammation. *Diabetes.* (2019)
- Delventhal R, O'Connor RM, Pantalia MM, et al. Dissection of central clock function in Drosophila through cell-specific CRISPR-mediated clock gene disruption. *Elife.* (2019)
- View More ...

Disclaimer

This product is for research use only and is not intended for therapeutic or diagnostic applications. Please contact a technical service representative for more information. All products of animal origin manufactured by Rockland Immunochemicals are derived from starting materials of North American origin. Collection was performed in United States Department of Agriculture (USDA) inspected facilities and all materials have been inspected and certified to be free of disease and suitable for exportation. All properties listed are typical characteristics and are not specifications. All suggestions and data are offered in good faith but without guarantee as conditions and methods of use of our products are beyond our control. All claims must be made within 30 days following the date of delivery. The prospective user must determine the suitability of our materials before adopting them on a commercial scale. Suggested uses of our products are not recommendations to use our products in violation of any patent or as a license under any patent of Rockland Immunochemicals, Inc. If you require a commercial license to use this material and do not have one, then return this material, unopened to: Rockland Inc., P.O. BOX 5199, Limerick, Pennsylvania, USA.